



**HAL**  
open science

# Sampling and Meshing Submanifolds in High Dimension

Jean-Daniel Boissonnat, Siargey Kachanovich, Mathijs Wintraecken

► **To cite this version:**

Jean-Daniel Boissonnat, Siargey Kachanovich, Mathijs Wintraecken. Sampling and Meshing Submanifolds in High Dimension. 2019. hal-02386169v1

**HAL Id: hal-02386169**

**<https://inria.hal.science/hal-02386169v1>**

Preprint submitted on 29 Nov 2019 (v1), last revised 29 Nov 2019 (v2)

**HAL** is a multi-disciplinary open access archive for the deposit and dissemination of scientific research documents, whether they are published or not. The documents may come from teaching and research institutions in France or abroad, or from public or private research centers.

L'archive ouverte pluridisciplinaire **HAL**, est destinée au dépôt et à la diffusion de documents scientifiques de niveau recherche, publiés ou non, émanant des établissements d'enseignement et de recherche français ou étrangers, des laboratoires publics ou privés.

# Sampling and Meshing Submanifolds in High Dimension

**Jean-Daniel Boissonnat**

Université Côte d’Azur, INRIA  
[Sophia-Antipolis, France]  
jean-daniel.boissonnat@inria.fr

**Siargey Kachanovich**

Université Côte d’Azur, INRIA  
[Sophia-Antipolis, France]  
siargey.kachanovich@inria.fr

**Mathijs Wintraecken**

IST Austria  
[Klosterneuburg, Austria]  
m.h.m.j.wintraecken@gmail.com

---

## 1 — Abstract

2 This paper presents a rather simple tracing algorithm to sample and mesh an  $m$ -dimensional sub-  
3 manifold of  $\mathbb{R}^d$  for arbitrary  $m$  and  $d$ . We extend the work of Dobkin et al. to submanifolds of  
4 arbitrary dimension and codimension. The algorithm is practical and has been thoroughly invest-  
5 igated from both theoretical and experimental perspectives. The paper provides a full description  
6 and analysis of the data structure and of the tracing algorithm. The main contributions are :  
7 1. We unify and complement the knowledge about Coxeter and Freudenthal-Kuhn triangulations.  
8 2. We introduce an elegant and compact data structure to store Coxeter or Freudenthal-Kuhn  
9 triangulations and describe output sensitive algorithms to compute faces and cofaces or any sim-  
10 plex in the triangulation. 3. We present a manifold tracing algorithm based on the above data  
11 structure. We provide a detailed complexity analysis along with experimental results that show  
12 that the algorithm can handle cases that are far ahead of the state-of-the-art.

**2012 ACM Subject Classification** Theory of computation → Computational geometry

**Keywords and phrases** Coxeter triangulation, Kuhn triangulation, permutahedron, PL-approx-  
imations, isomanifolds

**Funding** The research leading to these results has received funding from the European Research  
Council (ERC) under the European Union’s Seventh Framework Programme (FP/2007-2013)  
/ ERC Grant Agreement No. 339025 GUDHI (Algorithmic Foundations of Geometry Under-  
standing in Higher Dimensions) and the European Union’s Horizon 2020 research and innovation  
programme under the Marie Skłodowska-Curie grant agreement No. 754411.

**Acknowledgements** We thank Dominique Attali (CNRS), Arijit Ghosh (ISI), Vincent Pilaud  
(École polytechnique), and Aurélien Alvarez (ENS Lyon) for their comments and suggestion. We  
finally thank all former and current members of Datashape (formerly Geometrica) and Hebert  
Edelsbrunner’s group for the stimulating environment in which the research was conducted.

**Lines** 500



© Jean-Daniel Boissonnat, Siargey Kachanovich, and Mathijs Wintraecken;  
licensed under Creative Commons License CC-BY

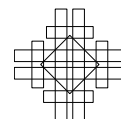
35th International Symposium on Computational Geometry (SoCG 2020).

Editors: ???; Article No. 00; pp. 00:1–00:23



Leibniz International Proceedings in Informatics

LIPIC Schloss Dagstuhl – Leibniz-Zentrum für Informatik, Dagstuhl Publishing, Germany



13 **1 Introduction**

14 This paper presents a rather simple algorithm to sample and mesh an  $m$ -dimensional sub-  
 15 manifold of  $\mathbb{R}^d$  for arbitrary  $m$  and  $d$ . This fundamental problem finds applications in  
 16 various fields like numerical analysis (to solve nonlinear differential equations) [3], dynam-  
 17 ical systems (to approximate invariant manifolds) [39, 28]), chemistry (to study the energy  
 18 landscape of molecules) [34], robotics (to describe the configuration space of mechanical sys-  
 19 tems) [31], computer vision and graphics (to visualize time-varying and higher dimensional  
 20 data) [5, 35].

21 **State-of-the-art.** The problem of triangulating differentiable manifolds has a long history  
 22 in Mathematics dating back to the work of Cairns [12], Whitehead [44] and Whitney[45].  
 23 More recently, the problem has received a lot of attention for surfaces of  $\mathbb{R}^3$  in the Compu-  
 24 tational Geometry and Computer Graphics communities. Among the widely used methods  
 25 are the Marching cube algorithm [42] and Delaunay refinement [14]. In higher dimensions,  
 26 some early work has been published in Applied Mathematics [1, 22, 39]. A slightly more  
 27 recent paper by Dobkin et al. [21] attracted the interest of the Computer Graphics com-  
 28 munity to Coxeter triangulations and their potential use for contour tracing. Although the  
 29 authors only considered the case of curves ( $m = 1$ ), it was claimed that the method could  
 30 be “immediately generalized” to submanifolds of higher codimensions. However there has  
 31 been only few works in that direction. This situation might be explained by the fact that  
 32 extending the Marching cube algorithm to higher dimensions seems infeasible due to the  
 33 large number of configurations that should be stored in a lookup table, and that no efficient  
 34 data structure was known to store and query triangulations in high dimensions. The most  
 35 recent work we are aware of is the work of Bhaniramka *et al.* [5] which is limited to hyper-  
 36 surfaces ( $m = d - 1$ ) and the work of Min [35]. Min’s method applies to submanifolds of  
 37 any dimension and codimension. It uses an ambient triangulation instead of a cubical grid  
 38 (the same Freudenthal-Kuhn triangulation used in this paper). However, in their analysis,  
 39 they consider  $d$  as a constant and only report experimental results in dimensions 3 and 4.

40 The problem we consider is also related to the problem of *manifold reconstruction* from  
 41 point samples [13, 7, 6]. A major difference however is that in manifold reconstruction, a  
 42 sample is given as input while here we have to construct the sample using an oracle that  
 43 queries the manifold. *Manifold sampling* is another related problem which is of fundamental  
 44 algorithmic significance in statistics. Yet, not much is known beyond the convex case and  
 45 the case of hypersurfaces ( $m = d - 1$ ) [20, 36].

46 **Contributions.** This paper is the first of a series of related papers to fill the gap. In this  
 47 paper, we extend the work of Dobkin et al. [21] to submanifolds of arbitrary codimension.  
 48 The algorithm is practical and has been thoroughly investigated from theoretical and ex-  
 49 perimental perspectives. This paper provides a full description and analysis of the data  
 50 structure and of the tracing algorithm.

51 Guarantees on output of the the algorithm are established in two companion papers, one  
 52 for the case of isomanifolds [10] and one for general smooth submanifolds [8]. Specifically, for  
 53 isomanifolds we prove [10] that the output is a PL-manifold that has the same topology type  
 54 as  $\mathcal{M}$ , and whose Fréchet distance to  $\mathcal{M}$  is small. Implementation details and experimental  
 55 results will be discussed in [9]. The case of submanifolds with boundaries and, more generally,  
 56 of stratified manifolds can be handled in very much the same way [9, 10].

57 The content of this paper is as follows. In Section 2, we first discuss Freudenthal-Kuhn  
 58 and Coxeter triangulations, the latter exclusively of type  $\tilde{A}_d$ . These triangulations have  
 59 different origins. Coxeter triangulations derive from geometric group theory, in particular

60 affine Weyl groups. Freudenthal-Kuhn triangulations are combinatorial by nature. Both  
 61 triangulations are the same up to a linear transformation, as noted by [21] and fully proved  
 62 in the appendix. This allows us to use on one hand the nice geometric properties of Coxeter  
 63 triangulations of type  $\tilde{A}_d$ , where each simplex is very well shaped (large volume compared to  
 64 longest edge length) and all simplices are identical up to reflections, and on the other hand  
 65 the simple combinatorial definitions of the Freudenthal-Kuhn triangulation. Although most  
 66 ideas in this section were known prior to this work, they were disseminated in many different  
 67 areas and difficult to access. We elucidate those ideas, provide full proofs and combine them  
 68 so as to extend them to arbitrary dimensions when necessary.

69 We then introduce a data structure to compactly store Coxeter or Freudenthal-Kuhn  
 70 triangulations. The data structure is an elegant and efficient representation of the combin-  
 71 atorial structure of those triangulations. We present a point location algorithm and describe  
 72 output sensitive algorithms for computing faces and cofaces of simplices of all dimensions in  
 73 the triangulation.

74 In Section 3, we present a submanifold tracing algorithm based on the above data struc-  
 75 ture. The algorithm works for smooth submanifolds of any dimension and codimension.  
 76 Starting from a given seed point, the algorithm probes the manifold using an oracle and  
 77 outputs both a sample and a PL approximation of the manifold. A distinctive property  
 78 of our algorithm, when compared to previous methods that work for submanifolds of ar-  
 79 bitrary dimension and codimension [1, 35], is that its complexity depends mostly on the  
 80 intrinsic dimension of the manifold (see Theorem 24 for a precise statement). Furthermore,  
 81 using dimensionality reduction techniques, we can completely remove the dependency of  
 82 the result on the ambient dimension (Theorem 26). The algorithm is quite simple and our  
 83 implementation can handle cases that are far beyond what was possible before (Section 4).

## 84 2 Coxeter-Freudenthal-Kuhn triangulations

### 85 2.1 Permutahedra

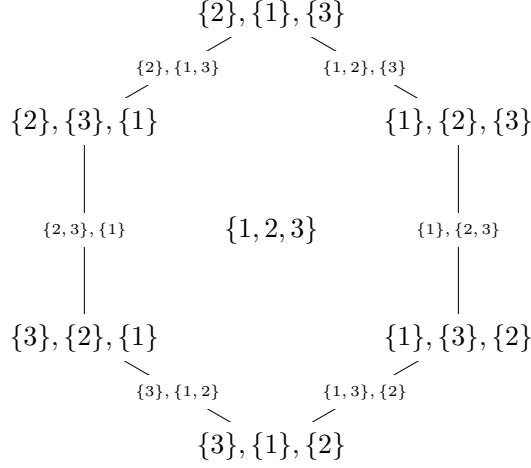
86 We write  $[k] = \{1, \dots, k\}$  and  $[k, l] = \{k, \dots, l\}$ .

87 ► **Definition 1** (Permutahedron). A  $d$ -permutahedron is a  $d$ -dimensional polytope, which is  
 88 the convex hull  $\mathcal{P}$  of all points in  $\mathbb{R}^{d+1}$ , the coordinates of which are permutations of  $[d+1]$ .  
 89 Formally, this convex hull can be written as:  $\mathcal{P} = \text{conv}\{(\sigma(1), \dots, \sigma(d+1)) \in \mathbb{R}^{d+1} \mid \sigma \in \mathfrak{S}_{d+1}\}$ ,  
 90 where  $\mathfrak{S}_{d+1}$  denotes the set of permutations of  $[d+1]$ .

91  $\mathcal{P}$  is at most  $d$ -dimensional since all its vertices lie on the hyperplane of equation  
 92  $\sum_{i=1}^{d+1} x^i = \frac{d(d+1)}{2}$ . Moreover, it can be shown that there are  $d+1$  affinely independent  
 93 vertices in  $\mathcal{P}$ , proving that  $\mathcal{P}$  is exactly  $d$ -dimensional (see for example [33, Lemma 3.4]).  
 94 The facial structure of  $\mathcal{P}$  is best described in terms of ordered partitions [46].

95 ► **Definition 2** (Ordered partition). Let  $T$  be a finite non-empty set,  $|T|$  its cardinality, and  
 96  $l \leq |T|$  a positive integer. An *ordered partition* of  $T$  in  $l$  parts is an ordered collection of  $l$   
 97 subsets  $\omega = (\omega_1, \dots, \omega_l)$ , such that  $\omega_i \subseteq T$  and  $\{\omega_1, \dots, \omega_l\}$  is a partition of  $T$ . The  $\omega_i$   
 98 are called the *parts*. We write  $OP_l[d]$  for the set of ordered partitions of  $[d]$  with  $l$  parts and  
 99 just  $OP[d]$  for the set of all ordered partitions of  $[d]$ .

100 ► **Definition 3** (Refinement). Let  $\omega$  and  $\varpi$  be two ordered partitions of  $[d+1]$  in  $k$  parts  
 101 and  $l$  parts respectively, with  $1 \leq k \leq l \leq d+1$ . We say that  $\varpi$  is a *refinement* of  
 102  $\omega$  if there exist positive integers  $a_1, \dots, a_k$  such that:  $(\varpi_1, \dots, \varpi_{a_1})$  is an ordered parti-  
 103 tion of  $\omega_1$  in  $a_1$  parts,  $(\varpi_{a_1+1}, \dots, \varpi_{a_1+a_2})$  is an ordered partition of  $\omega_2$  in  $a_2$  parts,  $\dots$ ,  
 104  $(\varpi_{a_1+\dots+a_{k-1}+1}, \dots, \varpi_{a_1+\dots+a_k})$  is an ordered partition of  $\omega_k$  in  $a_k$  parts.



111 ■ **Figure 1** The 2-permutahedron and the ordered partitions associated to its faces.

105 ► **Lemma 4** (Facial structure of the permutahedron, Theorem 3.6 of [33]). *The faces of a  $d$ -*  
 106 *permutahedron are in bijection with the ordered partitions of the set  $[d + 1]$ . More precisely,*  
 107 *the  $l$ -faces of  $\mathcal{P}$  correspond to ordered partitions of  $[d + 1]$  into  $d + 1 - l$  parts  $(\omega_1, \dots, \omega_{d+1-l})$*   
 108 *such that all coordinates in  $\omega_i$  are smaller than all coordinates in  $\omega_j$  for  $i < j$ . If  $\sigma$  and*  
 109  *$\tau$  are two faces of a  $d$ -permutahedron,  $\sigma$  is a subface of  $\tau$  (noted  $\sigma \subseteq \tau$ ) if and only if the*  
 110 *ordered partition associated to  $\sigma$  is a refinement of the ordered partition associated to  $\tau$ .*

112 ► **Corollary 5** (Corollary 3.15 of [33] and Theorem 3 of [37]). *The number of  $(d - l)$ -dimensional*  
 113 *faces in a  $d$ -permutahedron is  $(l + 1)! S(d + 1, l + 1)$ , where  $S(\cdot, \cdot)$  is the Stirling number of*  
 114 *the second kind. It is bounded by  $2^{2(d+1) \log(l+1)}$ .*

115 ► **Corollary 6.** *The number of vertices of a  $k$ -face of a  $d$ -permutahedron is at most  $(k + 1)!$*

116 ► **Lemma 7.** *The number of facets of an  $l$ -face  $\sigma$  of a  $d$ -permutahedron is  $O(2^l)$ .*

117 Proofs of the previous two corollaries are added in Appendix B for completeness.

## 118 2.2 Freudhental-Kuhn triangulation

119 The Freudhental-Kuhn (FK for short) triangulation is obtained from the  $d$ -grid, i.e. the  
 120 unit cubical tessellation of  $\mathbb{R}^d$  that consists of copies of the unit  $d$ -cube along the integer  
 121 lattice  $\mathbb{Z}^d$ . By triangulating each  $d$ -cube in the grid in an appropriate way to be described  
 122 now, we obtain the FK-triangulation of  $\mathbb{R}^d$ .

123 ► **Definition 8.** Let  $x \in \mathbb{R}^d$  and write  $z^i = x^i - \lfloor x^i \rfloor$ . We denote by  $e_1, \dots, e_d$  the basis  
 124 vectors and introduce, for reasons that will be clear later, the extra vector  $e_{d+1} = -\sum_{i=1}^d e_i$ .  
 125 We introduce the convention that  $z^{d+1} = 0$ . We associate to  $x$  the ordered partition  $\omega =$   
 126  $(\omega_1, \dots, \omega_{l+1})$  of  $[d + 1]$  where the  $\omega_i$  are obtained by sorting the  $z^i$  in decreasing order.  
 127 Specifically, with  $\omega_i = \{\omega_i(1), \dots, \omega_i(m_i)\}$ , we have

$$128 \quad 1 > z^{\omega_1(1)} = \dots = z^{\omega_1(m_1)} > \dots > z^{\omega_l(1)} = \dots = z^{\omega_l(m_l)} > z^{\omega_{l+1}(1)} = \dots = z^{\omega_{l+1}(m_{l+1})} = 0. \quad (1)$$

129 ► **Lemma 9.** *Suppose that  $\omega = (\omega_1, \dots, \omega_{l+1})$  is an ordered partition of  $[d + 1]$  and let*  
 130  *$\sigma = \{v_0, \dots, v_l\}$  be the  $l$ -simplex whose vertices are the points*

$$131 \quad v_0 = (\lfloor x^1 \rfloor, \dots, \lfloor x^d \rfloor), \quad v_i = v_{i-1} + \sum_{i \in \omega_i} e_i \quad i = 1, \dots, l. \quad (2)$$

132 *Then  $x$  is a point in the relative interior of  $\sigma$  if and only if  $z^i = x^i - \lfloor x^i \rfloor$ ,  $i = 1, \dots, d + 1$*   
 133 *(with, as above,  $z^{d+1} = 0$  and  $d + 1 \in \omega_{l+1}$ ), satisfy (1).*

134 **Proof.** Because the whole problem is translation invariant, we assume that  $v_0 = 0$  without  
 135 loss of generality, so that the expressions are shorter. Using barycentric coordinates,  $z \in \sigma$   
 136 can be written as

$$137 \quad z = \sum_{i=0}^l \lambda_i v_i = \sum_{i=0}^l \lambda_i \sum_{k=1}^i \sum_{j \in \omega_i} e_j$$

$$138 \quad = \lambda_l \left( \sum_{k \in \omega_l} e_k \right) + (\lambda_l + \lambda_{l-1}) \left( \sum_{k \in \omega_{l-1}} e_k \right) + \dots + (\lambda_l + \dots + \lambda_1) \left( \sum_{k \in \omega_1} e_k \right), \quad (3)$$

139 for some  $\lambda_i > 0$  satisfying  $\sum_{i=0}^l \lambda_i = 1$ . We write

$$140 \quad \alpha_{\omega_l(1)} = \dots = \alpha_{\omega_l(m_l)} = \lambda_l$$

$$141 \quad \vdots$$

$$142 \quad \alpha_{\omega_1(1)} = \dots = \alpha_{\omega_1(m_1)} = \lambda_l + \dots + \lambda_1 \quad (4)$$

143 By construction  $\alpha_{\omega_i(j)}$  is the  $\omega_i(j)$ th coordinate of  $z$ , denoted by  $z^{\omega_i(j)}$ , while all coordinates  
 144  $z^{\omega_{l+1}(1)}, \dots, z^{\omega_{l+1}(m_{l+1})}$  are zero, because  $e_{\omega_{l+1}(i)}$  does not occur in (3), for all  $i$ . Moreover,  
 145 because  $\lambda_l + \dots + \lambda_i > \lambda_l + \dots + \lambda_{i-1}$ , we see that (1) is satisfied.

146 Conversely, given a point  $z$  such that its coordinates satisfy (1), we can read of its  
 147 barycentric coordinates with respect to the  $v_i$ , as defined by (2), from (4). ◀

148 ► **Theorem 10.** *The equivalence classes of the points of  $\mathbb{R}^d$  with a same ordered partition*  
 149 *are the simplices of a triangulation of  $\mathbb{R}^d$  called the FK-triangulation.*

150 **Proof.** Lemma 9 implies that:

- 151 ■ Any face of a simplex in the FK-triangulation also lies in the FK-triangulation.
- 152 ■ The intersection of two simplices in the FK-triangulation also lie in the FK-triangulation.
- 153 ■ For any point  $x \in \mathbb{R}^d$ , there is a unique simplex  $\sigma$  such that  $x$  lies in the relative interior  
 154 of  $\sigma$ . Because  $x$  has uniquely defined barycentric coordinates with respect to the vertices  
 155 of  $\sigma$  it is mapped to a unique point in  $\sigma$ .

156 Hence the partition we have defined is a well-defined triangulation of  $\mathbb{R}^d$ . ◀

157 ► **Remark.** We note that, by construction,  $v_0$  in Lemma 9 is the smallest vertex of  $\sigma$  in  
 158 the lexicographical order. Lemma 9 also implies an observation of Freudenthal [25]: all  
 159  $d$ -simplices in the FK-triangulation can be described by monotone paths along the edges  
 160 of the cube from vertex  $(0, \dots, 0) + v_0$  to vertex  $(1, \dots, 1) + v_0$ . Conversely, any monotone  
 161 path along the edges of the cubes from  $(0, \dots, 0) + v_0$  to  $(1, \dots, 1) + v_0$  gives a simplex in  
 162 the FK-triangulation.

163 **Cycles and the permutahedron.** This monotone path can be made into a cycle using the  
 164 extra vector  $e_{d+1}$ , introduced by Eaves [22], because by construction  $v_0 = v_l + \sum_{i \in \omega_{l+1}} e_i$ ,  
 165 with  $\omega$  as in Definition 8. Because it is a cycle, we can take any vertex of the cycle as a  
 166 starting point, which means that  $v_0$  no longer has a special role as a starting point of a  
 167 monotone edge walk. A cycle can now be represented by an ordered partition of  $[d+1]$ , for  
 168 which it is not longer necessary that  $d+1$  lies in  $\omega_{l+1}$ , and an (arbitrary) starting point.

169 We now formalize these general cyclical paths:

170 ► **Definition 11** (Permutahedral representation). Let  $(v_0, \omega) \in \mathbb{Z}^d \times OP_{l+1}[d]$ . To this pair  
 171 we associate a simplex  $\sigma^\omega = \{v_0 = v_0^\omega, v_1^\omega, \dots, v_l^\omega\}$  with

$$172 \quad v_i^\omega = v_{i-1}^\omega + \sum_{i \in \omega_i} e_i \quad i = 1, \dots, l. \quad (5)$$

173 We say that  $(v_0, \omega)$  is the permutahedral representation of the simplex  $\sigma^\omega$ . If  $d+1 \in \omega_{l+1}$   
 174 we say that  $(v_0, \omega)$  is the canonical permutahedral representation of  $\sigma^\omega$ . In this case,  $\sigma^\omega$  is a  
 175 simplex in the FK-triangulation in the cube of which  $v_0$  is the minimal vertex with respect  
 176 to the lexicographical order, as we have seen above. In Lemma 14 and Proposition 15 we'll  
 177 see that, more generally,  $\{(v_0, \omega) \mid \omega \in OP[d+1]\}$  is the star of  $v_0$  in the FK-triangulation,  
 178 where we identify simplices with their permutahedral representations.

179 ► **Definition 12** (Cyclic shifts). Let  $(v_0, \omega)$  be a permutahedral representation. We define  
 180 the cyclic shift of  $(v_0, \omega)$  of length  $k$  to the left as  $(v'_0, \omega')$ , where

$$181 \quad v'_0 = v_0 + \sum_{j=1}^k \sum_{i \in \omega_j} e_i \quad \omega'_j = \omega_{(j+k-1) \bmod (l+1)+1}. \quad (6)$$

182 Here we use the convention that the sum from 1 to 0 is empty. We write  $(v'_0, \omega') = (v_0, \omega) \oplus k$ .

183 ► **Lemma 13.** *The cyclic shift  $(v'_0, \omega') = (v_0, \omega) \oplus k$  defines the same simplex as  $(v_0, \omega)$ .*

184 **Proof.** Follows by inserting (6) in (5). ◀

185 We now prove that the all permutahedral representations for a fixed  $v_0$ , form the star of  
 186  $v_0$ . This is a crucial property that will be used to efficiently compute faces and cofaces and  
 187 traverse the triangulation.

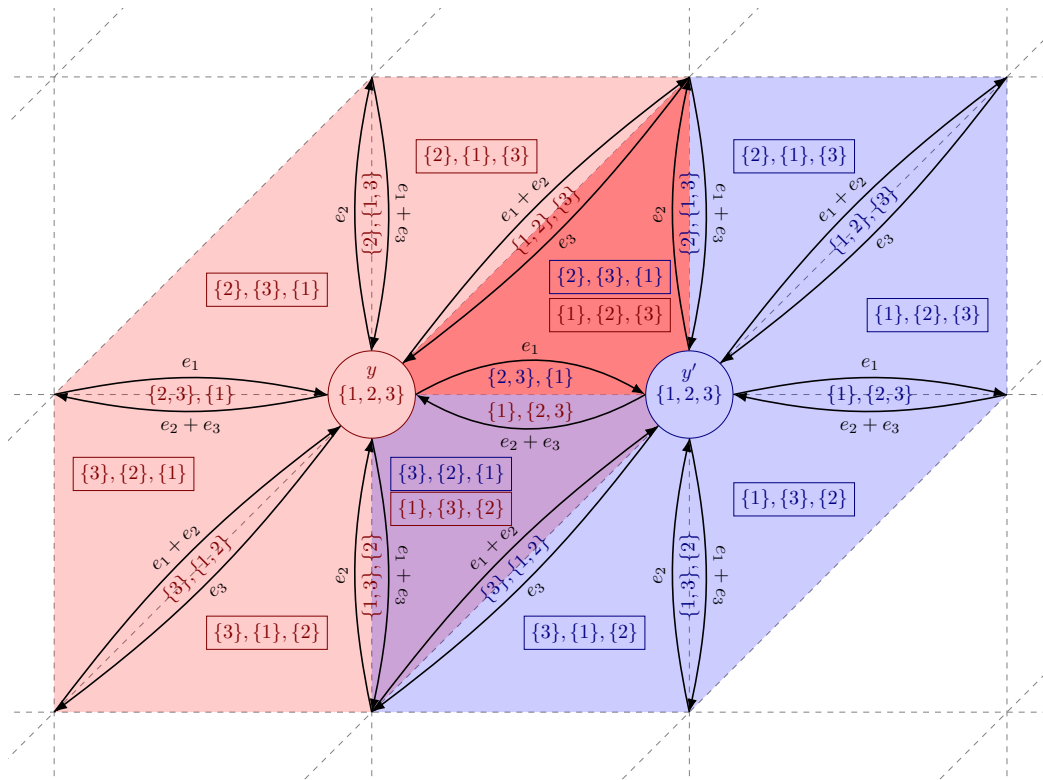
188 ► **Lemma 14.** *The set  $\{(v_0, \omega) \mid \omega \in OP[d+1]\}$ , where  $OP[d+1]$  is the set of all ordered  
 189 partitions of  $[d+1]$ , gives all the simplices in the star of  $v_0$  in FK-triangulation.*

190 **Proof.** Let  $(v_0, \omega)$ , with  $\omega \in OP_{l+1}[d+1]$ , be such that  $d+1 \in \omega_k$ . Let  $(v'_0, \omega') = (v_0, \omega) \oplus$   
 191  $(l-k+1)$ . By Definition 12 and Lemma 13,  $(v_0, \omega)$  and  $(v'_0, \omega')$  represent the same simplex.  
 192 Moreover  $d+1 \in \omega'_{l+1}$ , that is  $(v'_0, \omega')$  is a canonical permutahedral representation. This  
 193 implies that  $(v'_0, \omega')$  lies in the FK-triangulation by Lemma 9 and Theorem 10.

194 Conversely, suppose that  $(v'_0, \omega')$  is the canonical permutahedral representation of a  
 195 simplex in the star of  $v_0$ , that is there is some  $k$  such that  $v'_k = v_0$ , with  $v'_k$  as in (2). Then  
 196  $(v_0, \omega) = (v'_0, \omega') \oplus k$  is also a permutahedral representation of the same simplex. ◀

197 **Faces.** From (5) it is clear that merging two consecutive parts in the ordered partition  
 198  $\omega = (\omega_1, \dots, \omega_{l+1})$  corresponds to removing a vertex from the simplex, that is taking a  
 199 facet. Here we stress that we allow to merge  $\omega_1$ , and  $\omega_{l+1}$ , but in that case we have to  
 200 change the base point of the cycle to  $v_0 + \sum_{i \in \omega_1} e_i$ . For example, when looking at the two  
 201 dimensional example in Figure 2, we see that the edges that contain  $y$  in the red triangle with

202 permutahedral representation  $(y, (\{1\}, \{2\}, \{3\}))$  are  $(y, (\{1, 2\}, \{3\}))$ , and  $(y, (\{1\}, \{2, 3\}))$ .  
 203 The third edge of the red triangle is  $(y', (\{2\}, \{1, 3\}))$ . Generally, given an ordered partition  
 204  $\omega$  in  $l+1$  parts all  $(l-j)$ -faces can be found by merging  $j$  consecutive parts in  $\omega$  (for example  
 205 merging  $\omega_1$  with  $\omega_2$  and  $\omega_3$  with  $\omega_4$ ), where we allow  $\omega_{l+1}$  to merge with  $\omega_1$ , but in this  
 206 case we again need to change the base point.



207 ■ **Figure 2** The permutahedral representation of the simplices in the stars of vertices  $y$  and  $y'$ .

208 Because the combinatorial structure of the faces is compatible with the permutahedron,  
 209 Lemma 14 immediately gives:

210 ► **Proposition 15.** *The star of  $v_0$  is dual to a permutahedron (combinatorially).*

211 This proposition also explains the nomenclature permutahedral representation.

### 212 2.3 Basic operations

213 **Point location** Given a point  $x \in \mathbb{R}^d$  Lemma 9 tells us how to find the canonical permu-  
 214 tahedral representation of the simplex in which  $x$  is contained. The complexity of point  
 215 location is dominated by the sorting of the  $z^i = x^i - \lfloor x^i \rfloor$ , which takes  $O(d \log d)$  time and  
 216 requires  $O(d)$  space.

217 **Face computation.** Let  $\sigma$  be an  $l$ -simplex whose canonical permutahedral representation  
 218 is  $(v_0, \omega)$ , where  $\omega$  is an ordered partition of  $[d+1]$  into  $l+1$  parts. The computation of all  
 219  $k$ -faces of  $\sigma$  goes as follows. We use Ehrlich’s subset generation algorithm [24] to compute



220 all the subsets of  $k + 1$  elements from  $\{v_0, \dots, v_l\}$ . Let  $\tau = \{v_{m_0}, \dots, v_{m_k}\}$  be such a subset.  
 221  $\tau$  is a  $k$ -face of  $\sigma$ . We then compute the canonical permutahedral representation of all those  
 222  $k$ -faces  $\tau$ .

223 We first sort the  $m_i$  so that  $m_0 < \dots < m_k$  using counting sort. Then, the canonical  
 224 permutahedral representation  $(\tilde{v}'_0, \omega')$  of  $\tau$  is found by merging consecutive parts of  $\omega$  so as  
 225 to obtain  $k + 1$  parts as follows :

$$226 \quad v'_0 = v_{m_0} = v_0 + \sum_{j \in \omega_1} e_j + \dots + \sum_{j \in \omega_{m_0-1}} e_j$$

$$227 \quad \omega'_i = \omega_{m_{i-1}} \cup \dots \cup \omega_{m_i-1} \quad \text{for } i \in \{1, \dots, k\}$$

$$228 \quad \omega'_{k+1} = (\omega_1 \cup \dots \cup \omega_{m_0-1}) \cup (\omega_{m_k} \cup \dots \cup \omega_{l+1}).$$

229 The complexity of computing all subsets of  $k + 1$  vertices of  $\sigma$  using Ehrlich's algorithm  
 230 takes time  $O(k + s)$  where  $s = \binom{l+1}{k+1}$  is the number of subsets. Computing, for each such  
 231  $k$ -simplex its permutahedral representation takes  $O(d)$  time.

232 ► **Lemma 16.** *Let  $\sigma$  be an  $l$ -simplex in the FK-triangulation of  $\mathbb{R}^d$  given by its canonical*  
 233 *permutahedral representation. Computing the canonical permutahedral representations of*  
 234 *all its  $k$ -faces can be done in time  $O(ds)$ , where  $s = \binom{l+1}{k+1}$  is the number of  $k$ -faces of an  $l$*   
 235 *simplex. The space complexity of the algorithm is  $O(l)$  from the counting sort.*

236 **Coface computation.** Computing the faces of a simplex  $\sigma$  consisted in coarsifying its  
 237 ordered partition. The computation of cofaces is the reverse. Here we refine the ordered  
 238 partition. Specifically, if  $\sigma$  is a  $k$ -simplex represented by its canonical permutahedral repres-  
 239 entation  $(v_0, \omega)$ , and we want to compute its  $l$ -cofaces, we need to compute all refinements  
 240 of  $\omega$  into  $l + 1$  parts.

241 More precisely, we need to subdivide each  $\omega_i$  in  $a_i \leq |\omega_i|$  subparts so that  $\sum_{i=1}^{k+1} a_i = l+1$ .  
 242 This can be done in time proportional to the number  $k + 1$  of the generated subparts. We  
 243 then need to consider all the permutations of these subparts since we are interested in  
 244 ordered partitions. Using known algorithms by Walsh [41] and Ruskey and Savage [38], we  
 245 can compute all the ordered partitions associated to the  $l$ -cofaces of  $\sigma$  in time proportional  
 246 to the number of such cofaces. We thus obtain all the permutahedral representations  $(v_0, \omega')$   
 247 of all the  $l$ -cofaces of  $\sigma$ .

248 It is important to notice that all cofaces of  $\sigma$  have  $v_0$  as a vertex. However  $v_0$  is not  
 249 necessarily the minimal vertex of some of the computed cofaces. We thus have to identify  
 250 the minimal vertex of each computed coface and use cyclic shifts as in Lemma 14 to obtain  
 251 the canonical permutahedral representation of the coface.

252 ► **Lemma 17.** *Let  $\sigma$  be a  $k$ -simplex in the FK-triangulation of  $\mathbb{R}^d$  given by its permutahedral*  
 253 *representation. Computing the permutahedral representations of all its  $l$ -cofaces can be done*  
 254 *in time  $O(ds)$ , where  $s$  is the number of  $l$ -cofaces of a  $k$ -simplex in the FK-triangulation.*  
 255 *The space complexity of the algorithm is  $O(d)$ .*

## 256 2.4 Coxeter triangulations of type $\tilde{A}_d$

257 The Freudenthal-Kuhn triangulation is closely related to the Coxeter triangulation [18] of  
 258 type  $\tilde{A}_d$ . There are many equivalent ways to define the Coxeter triangulation of type  $\tilde{A}_d$ ,  
 259 see [11, 15, 29]. We recall the following:

260 ▶ **Definition 18.** Let  $P = \{(x^i) \in \mathbb{R}^{d+1} \mid \sum_i x^i = 0\}$  and consider the  $d$ -simplex with  
 261 vertices  $u_k$  in  $P$ .

$$262 \quad u_0 = \left(0^{\{d+1\}}\right) \quad u_k = \left(\left(-\frac{d+1-k}{d+1}\right)^{\{k\}}, \left(\frac{k}{d+1}\right)^{\{d+1-k\}}\right), \quad k \in [d],$$

263 where  $x^{\{k\}}$  denotes  $k$  consecutive coordinates  $x$ . The Coxeter triangulation of type  $\tilde{A}_d$  in  $P$   
 264 is found by consecutively reflecting the simplex in its faces.

265 The following lemma relates Coxeter and FK-triangulations and was first stated in [21].

266 ▶ **Lemma 19.** *The Freudenthal-Kuhn triangulation and Coxeter triangulation of type  $\tilde{A}_d$*   
 267 *are identical up to a linear transformation.*

268 A proof can be found in Appendix A. We will now call any triangulation of Euclidean space  
 269 that is the image of a Coxeter triangulation under a non-degenerate affine map a Coxeter-  
 270 Freudenthal-Kuhn triangulation, or CFK-triangulation for short. Moreover, we have

271 ▶ **Lemma 20** ([15]). *The Coxeter triangulation of type  $\tilde{A}_d$  is a Delaunay triangulation.*

272 We note that Proposition 15, together with Lemmas 19 and 20, give an alternative self-  
 273 contained proof of the known fact [17, Chapter 21, Section 3.F] (also proved in Appendix A  
 274 for completeness) that the Voronoi cell of a vertex in  $\tilde{A}_d$  is a (combinatorial) permutahedron.

275 The simplices in the Coxeter triangulation of type  $\tilde{A}_d$  have extremely good quality [15].  
 276 For example, the volume compared to the longest edge length to the  $d$ -th power is large. As  
 277 we will see, the exceptional quality of Coxeter improves the running of our algorithms.

## 278 2.5 Data structure for storing CFK-triangulations

279 To store an ambient CFK-triangulation for the manifold tracing algorithm in Section 3,  
 280 we use the following data structure. This data structure contains information on both the  
 281 combinatorial structure and the geometry of the triangulation. The combinatorics of the  
 282 triangulation is given through the canonical permutahedral representation of its simplices  
 283 and the algorithms from Section 2.2. The geometry of the triangulation is specified by the  
 284 affine transformation that maps the FK-triangulation of  $\mathbb{R}^d$  to the CFK-triangulation. The  
 285 affine transformation is given by a  $d \times d$  matrix  $\Lambda$  and a  $d$ -vector  $b$ .

286 ▶ **Remark.** Matrix  $\Lambda$  is used to compute the coordinates of the vertices of simplices and, for  
 287 the most useful cases in practice, needs not to be explicitly stored. For the FK-triangulation,  
 288  $\Lambda$  is the identity matrix and  $b = 0$ , therefore no storage is required. For the Coxeter  
 289 triangulation of type  $\tilde{A}_d$ , we can directly access the coordinates of vertices as given in  
 290 Definition 18.

## 291 3 Sampling and meshing submanifolds

292 In this section, we describe an algorithm that will compute a PL-approximation of an  $m$ -  
 293 submanifold of  $\mathbb{R}^d$  for arbitrary  $d$  and  $m \leq d$ . The algorithm can be considered as an  
 294 alternative to the Marching Cube algorithm [32] where the usual cubical grid is replaced by a  
 295 CFK — preferably the Coxeter — triangulation of the ambient space. Taking a triangulation  
 296 instead of a grid is a major advantage in high dimensions that has been recognized in the  
 297 pioneering works of Allgower and Schmidt [2] and of Dobkin et al. [21]. See also [35]. By  
 298 taking as a triangulation of the ambient space a CFK-triangulation, we keep two main  
 299 advantages of using grids: very limited storage and fast basic operations.

---

321 **Algorithm 1** Manifold tracing algorithm

---

321 **input** : Triangulation  $\mathcal{T}$  of  $\mathbb{R}^d$ , manifold  $\mathcal{M}$  of dimension  $m$ , seed point  $x_0 \in \mathcal{M}$   
322 **output**: Set  $\mathcal{S}$  of the simplices in  $\mathcal{T}$  of dimension  $k = d - m$  that intersect  $\mathcal{M}$   
323 Translate  $\mathcal{T}$  so that  $x_0$  coincides with the barycentre of a  $k$ -dimensional face  $\tau_0$  in  $\mathcal{T}$   
324 Initialize the queue  $\mathcal{Q}$  and the set  $\mathcal{S}$  with  $\tau_0$   
325 **while** the queue  $\mathcal{Q}$  is not empty **do**  
326     Pop a  $k$ -dimensional simplex  $\tau$  from  $\mathcal{Q}$   
327     **foreach** cofacet  $\phi$  of  $\tau$  **do**  
328         **foreach** facet  $\rho$  of  $\phi$  **do**  
329             **if**  $\rho$  does not lie in  $\mathcal{S}$  and intersects  $\mathcal{M}$  **then**  
330                 Insert  $\rho$  to the queue  $\mathcal{Q}$   
331                 Insert  $\rho$  together with the intersection point to the output set  $\mathcal{S}$

---

### 300 3.1 Manifold tracing algorithm

301 Let  $\mathcal{M}$  be an  $m$ -dimensional compact submanifold of the Euclidean space  $\mathbb{R}^d$ . Both  $m$   
302 and  $d$  are known but arbitrary and will be considered as parameters in the complexity  
303 analysis. The algorithm will use a CFK-triangulation  $\mathcal{T}$  of  $\mathbb{R}^d$ , which is stored using the  
304 data structure from Section 2.5. We assume that the manifold  $\mathcal{M}$  and the triangulation  $\mathcal{T}$   
305 satisfy a genericity hypothesis:

306 **► Hypothesis 21 (Genericity).** *The manifold has an empty intersection with all simplices of*  
307 *dimensions strictly lower than  $k$  in the triangulation  $\mathcal{T}$ . The intersection of the manifold*  
308  *$\mathcal{M}$  and any  $k$ -dimensional simplex in the triangulation  $\mathcal{T}$  is a single point.*

309 **► Remark.** It turns out [10] that for an isomanifold  $f^{-1}(0)$  it suffices to find the intersection  
310 points of  $f_{\text{PL}}^{-1}(0)$  with the  $k$ -simplices under very weak conditions. Here  $f_{\text{PL}}$  denotes the  
311 function that is linear on every simplex in  $\mathcal{T}$  and coincides with  $f$  on the vertices of  $\mathcal{T}$ . We  
312 stress that  $f_{\text{PL}}^{-1}(0)$  satisfies the genericity hypothesis with probability one.

313 We assume that we know a point on the manifold  $x_0 \in \mathcal{M}$ , from which the algorithm  
314 starts. If  $\mathcal{M}$  consists of multiple connected components, then a seed point per each connected  
315 component must be provided and we proceed in the same manner for each component. So  
316 we will assume for now that  $\mathcal{M}$  is connected.

317 In addition, we assume that the manifold  $\mathcal{M}$  can be accessed through an *oracle* that  
318 allows us to answer whether a  $k$ -simplex in the triangulation  $\mathcal{T}$  intersects the manifold  $\mathcal{M}$ .  
319 Here,  $k = d - m$  is the codimension of  $\mathcal{M}$ . In the following, we will refer to this oracle as  
320 the *intersection oracle*.

322 The algorithm is described as Algorithm 1. We first translate the coordinate frame so  
323 that  $x_0$  is the barycenter of a  $k$ -simplex of  $\mathcal{T}$  (any such simplex is fine). This simplex is put  
324 in the set  $\mathcal{S}$  of the simplices in  $\mathcal{T}$  of dimension  $k = d - m$  that intersect  $\mathcal{M}$ . Then, given such  
325 a simplex, we look at all its cofacets that have not been considered yet and consider all the  
326 facets of those cofacets that have not been considered yet. This can be done using a queue  
327  $\mathcal{Q}$  of simplices to consider. Each of these simplices is queried with the intersection oracle  
328 and, if it is found to intersect  $\mathcal{M}$ , it is added to  $\mathcal{S}$ . Upon termination,  $\mathcal{S}$  contains all the  
329  $k$ -dimensional simplices of  $\mathcal{T}$  that intersect  $\mathcal{M}$ . Since, by our genericity assumption, each  
330  $k$ -simplex in  $\mathcal{S}$  intersects  $\mathcal{M}$  in a single point,  $|\mathcal{S}|$  is also the size of the sample produced by  
331 our algorithm. A better approximation of the sample is of course possible if we have at our

332 disposal a more powerful intersection oracle that not only detects intersections but can also  
 333 compute intersection points between the simplices in  $\mathcal{S}$  and  $\mathcal{M}$ .

334 A polyhedron can be deduced from  $\mathcal{S}$  by taking the dual faces of the simplices in  $\mathcal{S}$ . A  
 335 more precise approximation can be obtained if, in addition to the intersection oracle, we  
 336 can also compute the intersection points  $\mathcal{S} \cap \mathcal{M}$ . This will be described in full detail in a  
 337 companion paper.

### 338 3.2 Complexity analysis

339 We can easily bound the complexity of the manifold tracing algorithm as a function of the  
 340 size of the output.

341 ► **Proposition 22.** *The time complexity of the algorithm is  $O(k2^m I |\mathcal{S}|)$ . where  $I$  is the time  
 342 complexity of one call of the intersection oracle and  $|\mathcal{S}|$  is the size of the output.*

343 **Proof.** The complexity of the initialization is  $O(d)$ . The complexity of each iteration of  
 344 the while loop consists of: computing the cofacets of the popped  $k$ -dimensional simplex in  
 345 the queue, computing facets of these cofacets and applying the intersection oracle on each  
 346 of these facets. From Lemma 7, the number of cofacets is  $O(2^m)$ . Each of these cofacets  
 347 has  $k + 2$  facets. Therefore, for each iteration of the while loop, the algorithm applies the  
 348 intersection oracle on  $O(k2^m)$  simplices. By using this observation and the complexities in  
 349 Lemmas 16 and 17, the total time complexity of each iteration of the while loop follows:

$$350 \quad O(d2^m) + O(dk2^m) + O(k2^m I) = O(k2^m(d + I)) = O(k2^m I).$$

351 Since there are  $|\mathcal{S}|$  iterations of the while loop, the result follows. ◀

352 We will now express the size of the output in terms of quantities that depend on the  
 353 manifold and the resolution of the triangulation.

► **Proposition 23** (Size of the output).

$$354 \quad |\mathcal{S}| \leq \frac{C}{\Theta \sqrt{m}} \left(\frac{2\pi e}{k}\right)^{k/2} \left(\frac{2}{\delta}\right)^m \text{vol}_m(\mathcal{M}) = O\left(2^{O(d \log d)} \frac{\text{vol}_m(\mathcal{M})}{\delta^m}\right).$$

355 where:

- 356 ■  $\text{vol}_m(\mathcal{M})$  is the  $m$ -dimensional volume of  $\mathcal{M}$ ,
- 357 ■  $\delta$  is the diameter of the  $d$ -simplices of  $\mathcal{T}$  and a measure of the resolution of  $\mathcal{T}$ ,
- 358 ■  $V$  is the volume of any  $d$ -simplex of  $\mathcal{T}$ , and  $\Theta = \frac{V}{\delta^d}$  its fatness,
- 359 ■  $C$  is a constant that does not depend on  $d$ ,  $m$  or  $\delta$ .

360 **Proof.** Let  $\mathcal{N}$  be the set of the  $d$ -dimensional cofaces of the simplices in  $\mathcal{S}$ , and let  $N$  be  
 361 the cardinality of  $\mathcal{N}$ . In the proof we will use constants  $C_1, C_2, C_3$  that are constants that  
 362 do not depend on  $d$ ,  $m$  nor  $\delta$ .

363 **Upper bound on  $N$ .** Write  $\mathcal{M}^\delta$  for the tubular neighbourhood of  $\mathcal{M}$  of radius  $\delta$ , i.e. the  
 364 set of points at distance at most  $\delta$  from  $\mathcal{M}$ . Since the  $d$ -dimensional simplices in  $\mathcal{N}$  have  
 365 pairwise disjoint interiors and all lie inside  $\mathcal{M}^\delta$ , we have

$$366 \quad N \cdot V \leq \text{vol}_d(\mathcal{M}^\delta). \tag{7}$$

## 00:12 Sampling and Meshing Submanifolds

367 According to the tube formula of Weyl [43, 26] and writing  $B_k$  for the volume of the unit  
368 ball of dimension  $k$ , there exists constants  $C_1$  and  $C_2$  such that

$$369 \quad \text{vol}_d(\mathcal{M}^\delta) \leq C_1 B_k \delta^k \text{vol}_m(\mathcal{M}) \leq C_2 \left(\frac{2\pi e}{k}\right)^{k/2} \delta^k \text{vol}_m(\mathcal{M}) \quad (8)$$

370 By combining the two inequalities (7) and (8), we get:

$$371 \quad N \leq \frac{\text{vol}_d(\mathcal{M}^\delta)}{V} \leq C_2 \left(\frac{2\pi e}{k}\right)^{k/2} \frac{\delta^k}{V} \text{vol}_m(\mathcal{M}) \leq C_2 \left(\frac{2\pi e}{k}\right)^{k/2} \frac{1}{\Theta} \frac{\text{vol}_m(\mathcal{M})}{\delta^m}. \quad (9)$$

372 where  $\Theta$  is the fatness of the simplices in the triangulation  $\mathcal{T}$ . Note that the dependency of  
373  $N$  on  $1/\delta$  is exponential in  $m$  but not in  $d$ .

374 **Upper bound on  $|\mathcal{S}|$ .** Now, we express  $|\mathcal{S}|$  in terms of  $N$ ,  $d$  and  $m$ . For this, we count  
375 the number INC of incidences of the  $k$ -dimensional simplices in  $\mathcal{S}$  and the  $d$ -dimensional  
376 simplices in  $\mathcal{N}$  in two ways:

$$377 \quad \sum_{\tau \in \mathcal{S}} |\text{cof}(\tau, d)| = \text{INC} = \sum_{\sigma \in \mathcal{N}} |\text{fac}(\sigma, k) \cap \mathcal{S}|. \quad (10)$$

378 The number of  $d$ -cofaces of a  $k$ -simplex is given by Corollary 6 applied to the dual Voronoi  
379 face of  $\tau$ . Hence there exists a constant  $C_3$  such that for any  $k$ -dimensional simplex  $\tau \in \mathcal{S}$ ,  
380 we have:

$$381 \quad |\text{cof}(\tau, d)| \geq C_3 \left(\frac{d}{m+1}\right)^{m+1}.$$

382 On the other hand, for each  $d$ -dimensional simplex  $\sigma \in \mathcal{N}$ , we have :

$$383 \quad |\text{fac}(\sigma, k) \cap \mathcal{S}| \leq |\text{fac}(\sigma, k)| = \binom{d+1}{m+1}.$$

384 Equation (10) becomes

$$385 \quad C_3 \left(\frac{d}{m+1}\right)^{m+1} |\mathcal{S}| \leq \sum_{\tau \in \mathcal{S}} |\text{cof}(\tau, d)| = \sum_{\sigma \in \mathcal{N}} |\text{fac}(\sigma, d) \cap \mathcal{S}| \leq \binom{d+1}{m+1} N,$$

386 from which we get using (9) that there exists a constant  $C$  such that

$$387 \quad |\mathcal{S}| \leq C \left(\frac{2\pi e}{k}\right)^{k/2} \frac{1}{\Theta} \text{vol}_m(\mathcal{M}) m^{-1/2} (2/\delta)^m.$$

388 **Bound on fatness.** The fatness term  $\Theta$  in the expression in Proposition 23 depends on  
389 the choice of the triangulation  $\mathcal{T}$ . The fatness  $\Theta_{CT}$  of the  $d$ -dimensional simplices in the  
390 Coxeter triangulation is given by (see [15])

$$391 \quad \frac{1}{\Theta_{CT}} = O\left(\frac{d^{(d+1)/2} d!}{2^d}\right) = O(2^{O(d \log d)}). \quad (11)$$

392 while the fatness  $\Theta_{FKT}$  of the  $d$ -dimensional simplices in the FK-triangulation of  $\mathbb{R}^d$  is given  
393 by (see [19])

$$394 \quad \frac{1}{\Theta_{FKT}} = O\left(d^{d/2} d!\right) = O(2^{O(d \log d)}). \quad (12)$$

395 Note that, in both cases,  $\Theta$  depends on the ambient dimension but not on  $\delta$ . Note also  
 396 that, while similar, the two bounds on the fatness differ by a factor  $2^d/\sqrt{d}$ . We thus expect  
 397 that using the Coxeter triangulation as the ambient triangulation will give a smaller output  
 398  $\mathcal{S}$  than the one we obtain using the Freudenthal-Kuhn triangulation. This is confirmed in  
 399 practice as shown in Section 4 (see Figure 6). ◀

400 We combine Propositions 22 and 23 in the following theorem.

401 ▶ **Theorem 24.** *The time complexity of the manifold tracing algorithm is  $2^{O(d \log d)} I \frac{\text{vol}_m(\mathcal{M})}{\delta^m}$ ,*  
 402 *where  $I$  is the time complexity of one call of the intersection oracle.*

403 **Cost of the oracle.** The cost of  $I$  depends on how the submanifold is given. As an example,  
 404 consider the case where  $\mathcal{M}$  is the PL-approximation of the zero set of a function  $f : \mathbb{R}^d \rightarrow \mathbb{R}^k$   
 405 and assume that evaluating  $f$  at any point  $x \in \mathbb{R}^d$  can be done in time polynomial in  $d$   
 406 (which, in particular, is true if each  $f^i$  is a polynomial in the coordinates of  $x$ ). Then  $I$   
 407 depends polynomially on  $d$  too. Indeed, consider a  $k$ -simplex  $\sigma$  of the triangulation on which  
 408 we call the intersection oracle and let  $H$  denote the  $m$ -flat that linearly interpolates  $f^{-1}(0)$   
 409 inside  $\sigma$ . To implement the oracle, we first evaluate  $f$  at the vertices of  $\sigma$ . We then compute  
 410 the barycentric coordinates of the (generically unique) point of intersection of the affine hull  
 411 of  $\sigma$  with  $H$ . Lastly, we check whether the barycentric coordinates are all non-negative (to  
 412 ensure that the intersection point lies inside  $\sigma$ ). It follows that the cost of the oracle is the  
 413 cost of evaluating  $f$  at the  $k + 1$  vertices of  $\sigma$  plus the cost of solving a linear system of  $k$   
 414 equations and  $k$  unknowns, which can be done in time  $O(k^{2.375})$ .

415 **Dimensionality reduction.** As seen from Proposition 23, the size  $\mathcal{S}$  of the output of  
 416 the algorithm, considered as a function of the resolution  $1/\delta$  of the triangulation, depends  
 417 exponentially on  $m$  (which is to be expected) and not on  $d$  (which is fortunate). Nevertheless,  
 418 the size of the output depends exponentially on  $d$ . This, in particular, means that the sample  
 419 constructed by the algorithm, although  $\delta$ -dense, is not guaranteed to be  $\mu\delta$  separated for  
 420 some constant  $\mu$ . In other words, the output sample is not a net of the manifold.

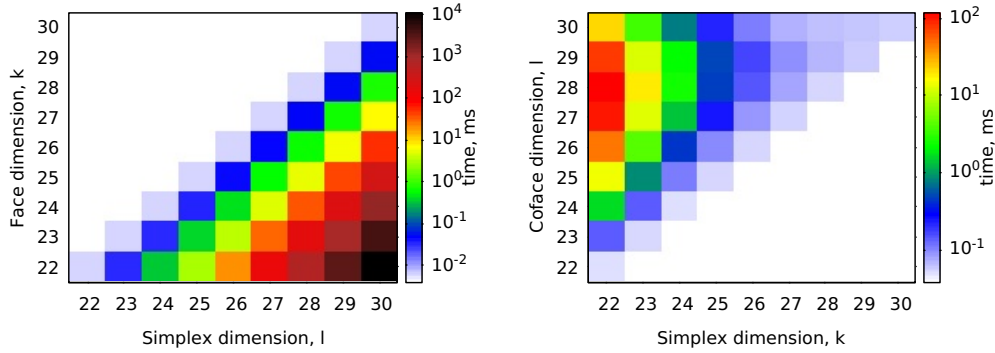
421 We can improve on the bound on  $\mathcal{S}$  by using dimensionality reduction techniques and,  
 422 specifically, a variant of the celebrated Johnson-Lindenstrauss lemma for manifolds. We  
 423 depart from our previous worst-case analysis by allowing some approximation factor  $\varepsilon$  and  
 424 tolerate a guarantee that holds only with high probability.

425 ▶ **Theorem 25** (Johnson-Lindenstrauss lemma for manifolds [16, 40]). *Pick any  $\varepsilon, \eta > 0$ ,*  
 426 *and let  $d' = \Omega\left(\frac{m}{\varepsilon^2} \log \frac{1}{\varepsilon} + \frac{1}{\varepsilon^2} \log \frac{\Gamma}{\delta}\right)$ , where  $\Gamma$  is a quantity that depends only on intrinsic*  
 427 *properties of  $\mathcal{M}$ . Let  $\Phi$  be a random affine subspace of dimension  $d'$ . Then, with probability*  
 428  *$> 1 - \eta$ , for all  $x, y \in \mathcal{M}$*

429 
$$(1 - \varepsilon) \sqrt{\frac{d'}{d}} \leq \frac{\|\Phi x - \Phi y\|}{\|x - y\|} \leq (1 + \varepsilon) \sqrt{\frac{d'}{d}}.$$

430 It follows that the image  $\Phi\mathcal{M}$  of  $\mathcal{M}$  will be a submanifold of dimension  $m$  embedded in  
 431  $\mathbb{R}^{d'}$ . One can now run the manifold tracing algorithm in  $\mathbb{R}^{d'}$  to sample and mesh  $\Phi\mathcal{M}$ .  
 432 The algorithm works as described before except that we need another oracle that, given a  
 433  $(d' - m)$ -simplex  $\sigma$  of the CFK-triangulation of  $\mathbb{R}^{d'}$ , decides whether its inverse image  $\Phi^{-1}\sigma$ ,  
 434 which is a  $(d - d')$ -dimensional flat strip in  $\mathbb{R}^d$ , intersects  $\mathcal{M}$  or not.

435 Due to the scaling factor  $\sqrt{d/d'}$ , the resolution of the triangulation in the low dimensional  
 436 plane has to be scaled by the same factor if one wants to satisfy a given sampling density  
 437 on  $\mathcal{M}$ . Since the geometry of the manifold (reach and volume) is also scaled in the same  
 438 way [23], the analysis of the algorithm will be unchanged. Theorem 24 shows that the



455 **Figure 3** On the left: comparison of the execution time of the face and the coface generation  
 456 algorithm for simplices of various dimensions in a CFK-triangulation of  $\mathbb{R}^{30}$ . Because the average  
 457 computation time of a face or coface is constant, the presented time is proportional to the number of  
 458 faces or cofaces of respective simplices.

439 output sample will have size  $O\left(2^{O(d' \log d')} \frac{\text{vol}_m(\mathcal{M})}{\delta^m}\right)$ . Since  $d'$  does not depend on the  
 440 ambient dimension  $d$  by Theorem 25, neither does the size of the output sample.

441 **► Theorem 26.** *Pick any  $\varepsilon, \eta > 0$ , and let  $d' = \Omega\left(\frac{m}{\varepsilon^2} \log \frac{1}{\varepsilon} + \frac{1}{\varepsilon^2} \log \frac{\Gamma}{\delta}\right)$ , where  $\Gamma$  is a  
 442 quantity that depends only on intrinsic properties of  $\mathcal{M}$ . Let  $\Phi$  be a random affine subspace  
 443 of dimension  $d'$ . Then, with probability  $> 1 - \eta$ , we can sample and mesh  $\mathcal{M}$  using the tracing  
 444 algorithm in  $\mathbb{R}^{d'}$  and the new oracle. The size of the output is  $O\left(2^{O(d' \log d')} \frac{\text{vol}_m(\mathcal{M})}{\delta^m}\right)$ .*

445 The previous theorem bounds the size of the output. The complexity of the new oracle  
 446 is the same as the complexity of the basic intersection oracle.

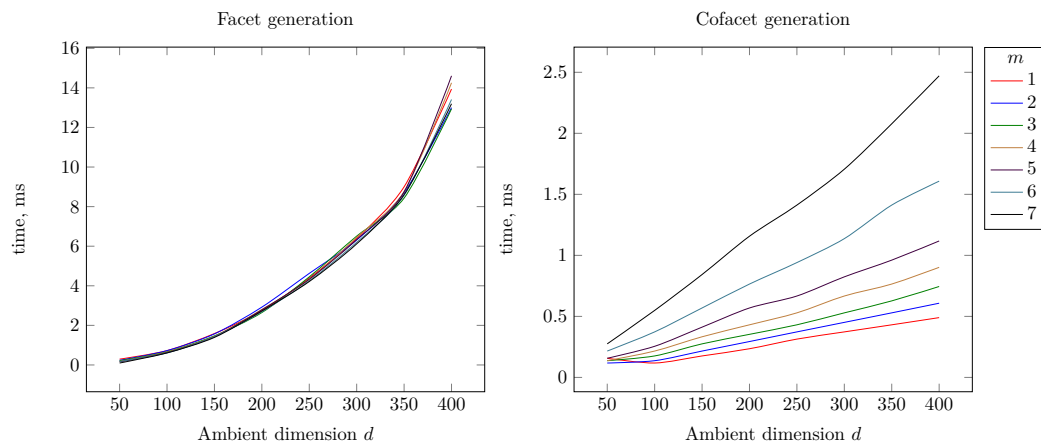
## 447 4 Experimental results

448 The data structure of Section 2 and the algorithm of Section 3 have been implemented in  
 449 C++. The code is robust and fast, and will be released soon in the GUDHI library [27]. Full  
 450 detail on the implementation, including the implementation of the oracle, will be reported  
 451 in a companion paper together with experimental results [9]. See also [30].

452 In this section, we explore the dependency of our C++ implementation of the data struc-  
 453 ture for the ambient CFK-triangulation and of the manifold tracing algorithm on the prop-  
 454 erties of the triangulation and of the input manifold.

### 461 Data structure.

462 In Figure 3, we present the time of generating all faces (on the left) and all cofaces (on the  
 463 right) of various dimensions of simplices in a CFK-triangulation of  $\mathbb{R}^{30}$  using algorithms  
 464 from Section 2.2. The presented execution time is averaged over 500 tests. Note that both  
 465 for face and coface generation algorithms, the execution time is proportional to the number  
 466 of computed elements. On average, these algorithms take time 0.001-0.002 ms per computed  
 467 face or coface, regardless of the dimensions of the input simplex and of the computed element.  
 468 In Figure 4, we further illustrate the particular case of facet and cofacet computation, which  
 469 is essential in the manifold tracing algorithm. We show the dependency of the execution  
 470 time on two parameters: the ambient dimension  $d$  and the codimension  $m$  of the input



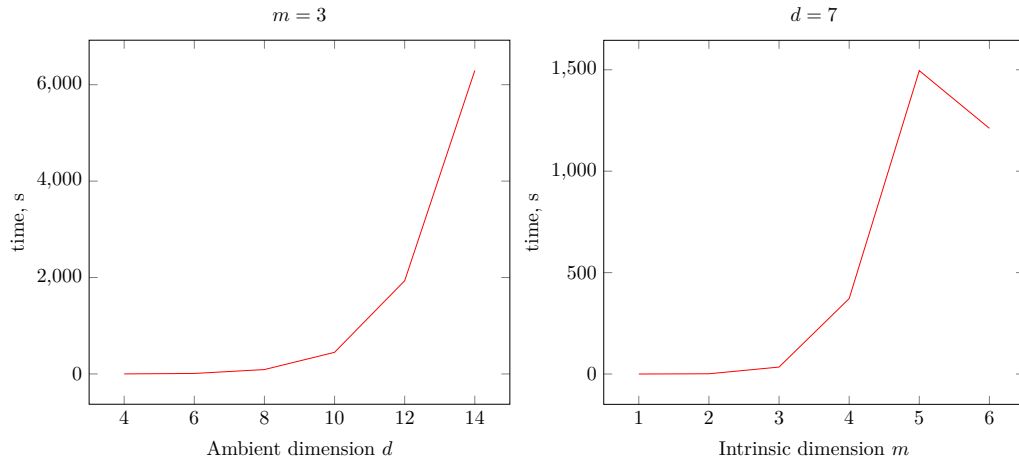
459 **Figure 4** Execution time of the facet and cofacet computation depending on the dimension  $d$  of  
 460 the triangulation and the codimension  $m$  of the input simplex.

471 simplex, which corresponds to the intrinsic dimension of the input manifold in the manifold  
 472 tracing algorithm.

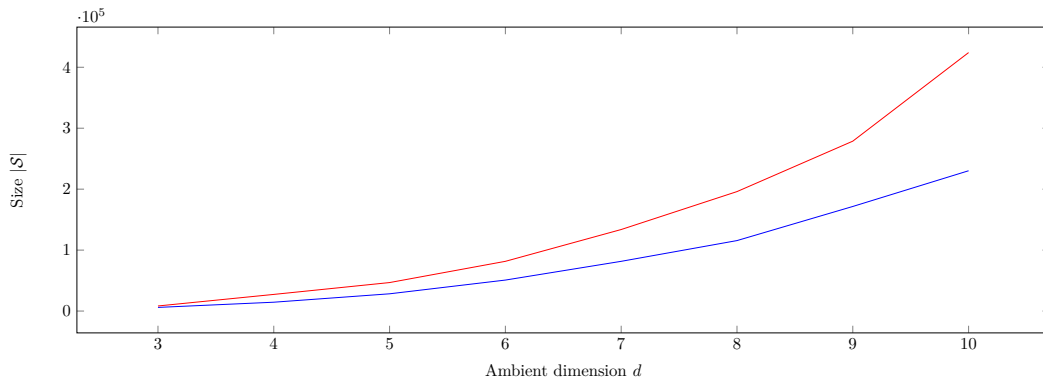
491 **Manifold tracing algorithm.**

492 We show the performance of our implementation of the manifold tracing algorithm for  
 493 various ambient and intrinsic dimensions in Figure 5. In Figure 6, we can see that using  
 494 Coxeter triangulation is beneficial in practice as it produces a smaller output in less time. In  
 495 Figure 7, we present a PL approximation of a two-dimensional flat torus without boundary  
 496 embedded in  $\mathbb{R}^{10}$  built by the manifold tracing algorithm. The algorithm can be easily  
 497 adapted to handle submanifolds with boundary. In Figure 8, we present the mesh obtained  
 498 by our algorithm on a portion of a flat torus embedded in  $\mathbb{R}^4$  and cut by a hypersphere.  
 499 Both surfaces in Figure 7 and 8 are rotated and translated in their respective ambient spaces  
 500 for visualization purposes. Note that there is no  $C^2$  embedding of the flat torus in  $\mathbb{R}^3$ .

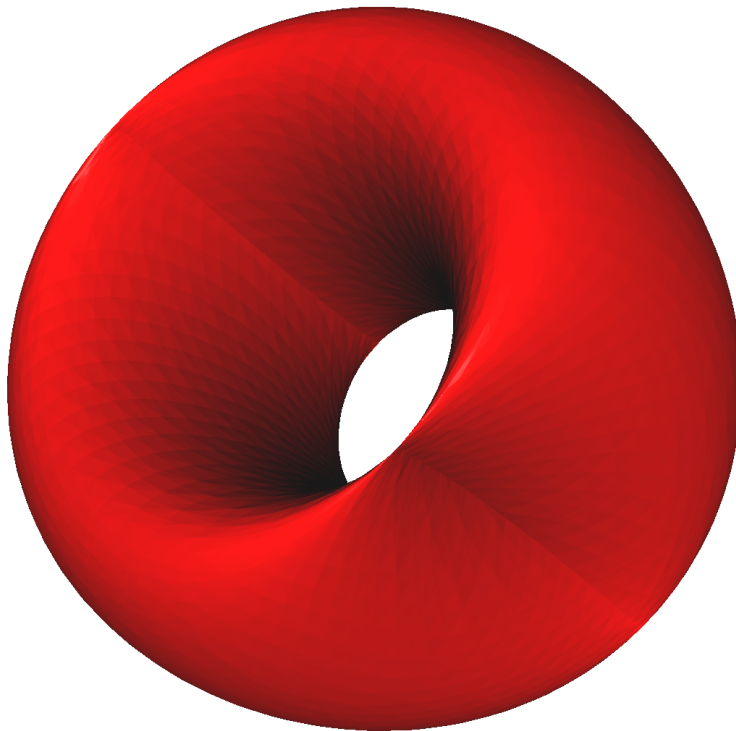




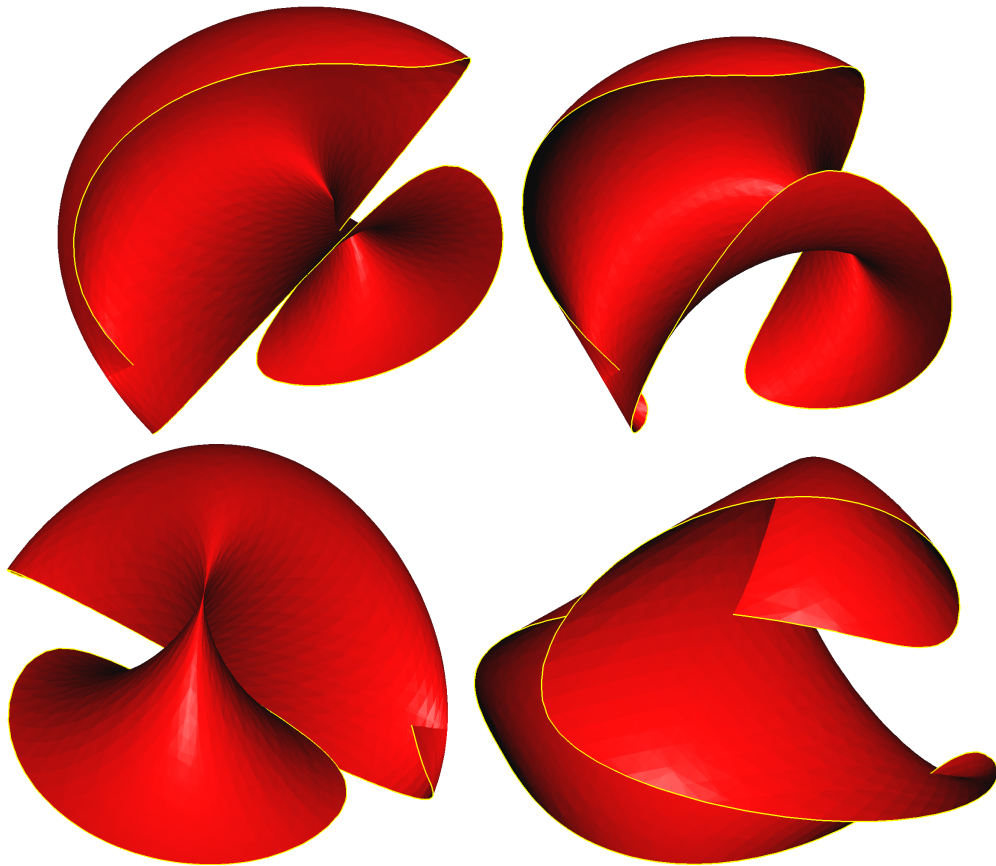
473 **Figure 5** The effect of the ambient dimension  $d$  and of the intrinsic dimension  $m$  on the compu-  
 474 tation time of the of the manifold tracing algorithm. The reconstructed manifold in the tests is the  
 475  $m$ -dimensional sphere embedded in  $\mathbb{R}^d$ . The ambient triangulation used is a Coxeter triangulation  
 476 of type  $\tilde{A}_d$ . The diameter of the full simplices is fixed for all  $d$ .



477 **Figure 6** Comparison of the size of the output of the manifold tracing algorithm using two types  
 478 of the ambient triangulation: a Coxeter triangulation of type  $\tilde{A}_d$  (in blue) and the Freudenthal-  
 479 Kuhn triangulation of  $\mathbb{R}^d$  (in red) with the same diameter  $0.07\sqrt{d}$  of  $d$ -dimensional simplices. The  
 480 reconstructed manifold is the 2-dimensional implicit surface “Chair” embedded in  $\mathbb{R}^d$  given by the  
 481 equations:  $(x_1^2 + x_2^2 + x_3^2 - 0.8)^2 - 0.4((x_3 - 1)^2 - 2x_1^2)((x_3 + 1)^2 - 2x_2^2) = 0$  and  $x_i = 0$  for  $i > 3$ .



482 ■ **Figure 7** The piecewise-linear approximation of a flat torus embedded in  $\mathbb{R}^{10}$  defined by the  
483 equations  $x_1^2 + x_2^2 = 1$  and  $x_3^2 + x_4^2 = 1$  and  $x_i = 0$  for  $i > 4$ , projected to  $\mathbb{R}^3$ . The ambient  
484 triangulation used is a Coxeter triangulation of type  $\tilde{A}_{10}$  with the diameter of the full-dimensional  
485 simplices 0.23. The output size  $|\mathcal{S}|$  is 509952. The execution time of the algorithm is 231s.



486 ■ **Figure 8** Four views of the flat torus in  $\mathbb{R}^4$  given by two equations  $x_1^2 + x_2^2 = 1$  and  $x_3^2 + x_4^2 = 1$  cut  
 487 by the hypersphere  $(x_1 - 1)^2 + x_2^2 + (x_3 - 1)^2 + x_4^2 = 4$ , projected to  $\mathbb{R}^3$ . The ambient triangulation used  
 488 is a Coxeter triangulation of type  $\tilde{A}_4$  with the diameter 0.15 of the full-dimensional simplices. The  
 489 reconstructed boundary is highlighted in yellow. The size  $|\mathcal{S}|$  of the piecewise-linear approximation  
 490 is 14779. The execution time of the algorithm is 1.84s.

501 ——— **References** ———

- 502 **1** Eugene Allgower and Kurt Georg. *Numerical continuation methods: an introduction*,  
503 volume 13. Springer Science & Business Media, 1990.
- 504 **2** Eugene Allgower and Phillip H. Schmidt. An algorithm for piecewise-linear approximation  
505 of an implicitly defined manifold. *SIAM journal on numerical analysis*, 22(2):322–346,  
506 1985.
- 507 **3** Luigi Ambrosio and Halil Mete Soner. Level set approach to mean curvature flow in  
508 arbitrary codimension. *J. Differential Geom.*, 43(4):693–737, 1996. URL: <https://doi.org/10.4310/jdg/1214458529>, doi:10.4310/jdg/1214458529.
- 509 **4** M. A. Armstrong. *Groups and Symmetry*. Springer, 1988.
- 510 **5** Praveen Bhaniramka, Rephael Wenger, and Roger Crawfis. Isosurfacing in higher dimen-  
511 sions. In *Proceedings of the conference on Visualization'00*, pages 267–273. IEEE Computer  
512 Society Press, 2000.
- 513 **6** Jean-Daniel Boissonnat and Arijit Ghosh. Manifold reconstruction using tangential  
514 Delaunay complexes. *Discrete & Computational Geometry*, 51(1):221–267, 2014.
- 515 **7** Jean-Daniel Boissonnat, Leonidas J. Guibas, and Steve Oudot. Manifold reconstruction  
516 in arbitrary dimensions using witness complexes. *Discrete & Computational Geometry*,  
517 42(1):37–70, 2009. URL: <https://doi.org/10.1007/s00454-009-9175-1>, doi:10.1007/  
518 s00454-009-9175-1.
- 519 **8** Jean-Daniel Boissonnat, Sargey Kachanovich, and Mathijs Wintraecken. Triangulating  
520 submanifolds: An elementary and quantified version of Whitney’s method. Preprint,  
521 December 2018. URL: <https://hal.inria.fr/hal-01950149>.
- 522 **9** Jean-Daniel Boissonnat, Sargey Kachanovich, and Mathijs Wintraecken. Tracing isoman-  
523 ifolds of arbitrary dimension and codimension. In preparation, December 2019.
- 524 **10** Jean-Daniel Boissonnat and Mathijs Wintraecken. The topological correctness of the PL-  
525 approximations of isomanifolds. Submitted to SoCG 2020, December 2019.
- 526 **11** Nicolas Bourbaki. Lie groups and Lie algebras. Chapters 4–6. Translated from the 1968  
527 French original by Andrew Pressley. *Elements of Mathematics*, 2002.
- 528 **12** S. S. Cairns. On the triangulation of regular loci. *Annals of Mathematics. Second Series*,  
529 35(3):579–587, 1934. doi:10.2307/1968752.
- 530 **13** S-W. Cheng, T. K. Dey, and E. A. Ramos. Manifold Reconstruction from Point Samples.  
531 In *Proc. ACM-SIAM Symp. Discrete Algorithms*, pages 1018–1027, 2005.
- 532 **14** Siu-Wing Cheng, Tamal K. Dey, and Jonathan Richard Shewchuk. *Delaunay Mesh Gen-*  
533 *eration*. Chapman and Hall / CRC computer and information science series. CRC Press,  
534 2013. URL: <http://www.crcpress.com/product/isbn/9781584887300>.
- 535 **15** Aruni Choudhary, Sargey Kachanovich, and Mathijs Wintraecken. Coxeter triangula-  
536 tions have good quality. Submitted, December 2017. URL: [https://hal.inria.fr/  
537 hal-01667404](https://hal.inria.fr/hal-01667404).
- 538 **16** Kenneth L. Clarkson. Tighter bounds for random projections of manifolds. In *Proceedings*  
539 *of the 24th ACM Symposium on Computational Geometry, College Park, MD, USA, June*  
540 *9-11, 2008*, pages 39–48, 2008. URL: <https://doi.org/10.1145/1377676.1377685>, doi:  
541 10.1145/1377676.1377685.
- 542 **17** J. H. Conway and N. J. A. Sloane. *Sphere-packings, Lattices, and Groups*. Springer-Verlag  
543 New York, Inc., New York, NY, USA, 1987.
- 544 **18** Harold S. M. Coxeter. Discrete groups generated by reflections. *Annals of Mathematics*,  
545 pages 588–621, 1934.
- 546 **19** Wolfgang A. Dahmen and Charles A. Micchelli. On the linear independence of multivariate  
547 B-splines, I. Triangulations of simplexes. *SIAM Journal on Numerical Analysis*, 19(5):993–  
548 1012, 1982.
- 549

- 550 20 Persi Diaconis, Susan Holmesand, and Mehrdad Shahshahani. Sampling from a manifold.  
551 *IMS Collections*, 2012.
- 552 21 David P. Dobkin, Allan R. Wilks, Silvio V. F. Levy, and William P. Thurston. Con-  
553 tour tracing by piecewise linear approximations. *ACM Transactions on Graphics (TOG)*,  
554 9(4):389–423, 1990.
- 555 22 B. Curtis Eaves. *A course in triangulations for solving equations with deformations*, volume  
556 234. Lecture Notes in Economics and Mathematical Systems, 1984.
- 557 23 Armin Eftekhari and Michael B. Wakin. What happens to a manifold under a bi-lipschitz  
558 map? *Discrete & Computational Geometry*, 57(3):641–673, 2017. URL: <https://doi.org/10.1007/s00454-016-9847-6>, doi:10.1007/s00454-016-9847-6.
- 560 24 Gideon Ehrlich. Loopless algorithms for generating permutations, combinations, and other  
561 combinatorial configurations. *Journal of the ACM (JACM)*, 20(3):500–513, 1973.
- 562 25 Hans Freudenthal. Simplicialzerlegungen von beschränkter flachheit. *Annals of Mathemat-*  
563 *ics*, pages 580–582, 1942.
- 564 26 Alfred Gray. Comparison theorems for the volumes of tubes as generalizations of the weyl  
565 tube formula. *Topology*, 21(2):201–228, 1982.
- 566 27 GUDHI Project. GUDHI Editorial Board. URL: <http://gudhi.gforge.inria.fr/doc/latest/>.
- 568 28 George Haller and Sten Ponsioen. Nonlinear normal modes and spectral submanifolds:  
569 existence, uniqueness and use in model reduction. *Nonlinear dynamics*, 86(3):1493–1534,  
570 2016.
- 571 29 James E. Humphreys. *Reflection groups and Coxeter groups*, volume 29. Cambridge uni-  
572 versity press, 1992.
- 573 30 Siargey Kachanovich. *Manifold meshing using Coxeter triangulations*. PhD thesis, Uni-  
574 versité Côte d’Azur, 2019.
- 575 31 S. M. LaValle. *Planning Algorithms*. Cambridge University Press, Cambridge, U.K., 2006.  
576 Available at <http://planning.cs.uiuc.edu/>.
- 577 32 William E. Lorensen and Harvey E. Cline. Marching cubes: A high resolution 3d surface  
578 construction algorithm. In *ACM siggraph computer graphics*, volume 21, pages 163–169.  
579 ACM, 1987.
- 580 33 M. Maes and B. Kappen. On the permutahedron and the quadratic placement problem.  
581 *Philips Journal of Research*, 46(6):267–292, 1992.
- 582 34 Shawn Martin, Aidan Thompson, Evangelos A Coutsias, and Jean-Paul Watson. Topology  
583 of cyclo-octane energy landscape. *The journal of chemical physics*, 132(23):234115, 2010.
- 584 35 Chohong Min. Simplicial isosurfacing in arbitrary dimension and codimension. *Journal of*  
585 *Computational Physics*, 190(1):295–310, 2003.
- 586 36 Hariharan Narayanan and Partha Niyogi. Sampling hypersurfaces through diffusion. In  
587 *12th Intl. Workshop on Randomization and Computation (RANDOM)*, 2008.
- 588 37 B.C. Rennie and A.J. Dobson. On Stirling numbers of the second kind. *Journal of Combin-*  
589 *atorial Theory*, 7(2):116 – 121, 1969. URL: <http://www.sciencedirect.com/science/article/pii/S0021980069800451>, doi:[https://doi.org/10.1016/S0021-9800\(69\)80045-1](https://doi.org/10.1016/S0021-9800(69)80045-1).
- 592 38 Frank Ruskey and Carla D. Savage. Gray codes for set partitions and restricted growth  
593 tails. *Australasian J. Combinatorics*, 10:85–96, 1994.
- 594 39 Michael J. Todd. *The computation of fixed points and applications*, volume 124. Lecture  
595 Notes in Economics and Mathematical Systems, 1976.
- 596 40 Nakul Verma. A note on random projections for preserving paths on a manifold. Technical  
597 Report Tech. Report CS2011-0971, UC San Diego, 2011.
- 598 41 Timothy R. Walsh. Loop-free sequencing of bounded integer compositions. *Journal of*  
599 *Combinatorial Mathematics and Combinatorial Computing*, 33:323–345, 2000.

600 42 Rephael Wenger. *Isosurfaces: geometry, topology, and algorithms*. AK Peters/CRC Press, 2013.  
 601  
 602 43 Hermann Weyl. On the volume of tubes. *American Journal of Mathematics*, 61(2):461–472, 1939.  
 603  
 604 44 J. H. C. Whitehead. On  $C^1$ -complexes. *Annals of Mathematics*, 41(4):809–824, 1940. URL: <http://www.jstor.org/stable/1968861>.  
 605  
 606 45 H. Whitney. *Geometric Integration Theory*. Princeton University Press, 1957.  
 607 46 G. M. Ziegler. *Lectures on Polytopes*. Graduate Texts in Mathematics. Springer New York, 2012. URL: <https://books.google.fr/books?id=xd25TXSSUcgC>.  
 608

609 **A Proofs for Section 2.4**

610 In this appendix we will prove that the Freudenthal-Kuhn triangulation is the Coxeter  
 611 triangulations of type  $\tilde{A}_d$  up to a linear transformation. We also prove that the Voronoi cell  
 612 of a vertex in a Coxeter triangulation of type  $\tilde{A}_d$  is a permutahedron.

613 For this we need to first recall an equivalent definition of the Coxeter triangulations of  
 614 type  $\tilde{A}_d$ : Any Coxeter triangulation can be defined as an hyperplane arrangement

615 
$$\mathcal{H} = \{H_{r,k} \mid r \in R_+, k \in \mathbb{Z}\},$$

616 where

617 
$$H_{u,k} = \{x \in \mathbb{R}^d \mid \langle x, u \rangle = k\},$$

618 and  $R_+$  denotes the set of *positive roots* of the Coxeter group. We will not recall the general  
 619 definition of positive roots, which can be found in for example [11, 29, 15], but use that for  
 620  $\tilde{A}_d$ , according to [11, Planche II],

621 
$$R_+ = \left\{ r_{i,j} = \sum_{l=i}^j s_l \mid 1 \leq i \leq j \leq d \right\},$$

622 with  $\{s_i\}$  the *simple roots* of the Weyl group  $A_d$  associated to the triangulation of type  $\tilde{A}_d$ .  
 623 For a discussion of the Weyl group we again refer to for example [11, 29, 15]. We also recall  
 624 the simple roots of  $A_d$ , which will be needed in the second proof. The simple roots of  $A_d$   
 625 (in the hyperplane  $P = \{(x^i) \in \mathbb{R}^{d+1} \mid \sum_i x^i = 0\} \subset \mathbb{R}^{d+1}$ ) are in turn:

626 
$$s_1 = e_1 - e_2, s_2 = e_2 - e_3, \dots, s_d = e_d - e_{d+1},$$

627 see [11]. We stress that these simple roots can be rescaled, permuted and rotated in  
 628 the hyperplane  $P$ . We note that one can easily rotate  $\mathbb{R}^d \subset \mathbb{R}^{d+1}$  given by the first  $d$   
 629 basis vectors into  $P$ . The matrix in  $\text{SO}(d+1)$  of this transformation has as first  $d$  rows  
 630  $((1/\sqrt{i^2+i})^{\{i\}}, -i/\sqrt{i^2+i}, 0^{\{d-i-1\}})$  and the final row  $((1/\sqrt{d+1})^{\{d+1\}})$ , where  $c^{\{k\}}$  de-  
 631 notes  $k$  consecutive coordinates equal to  $c$ . We will not use this transformation because it  
 632 complicates the expressions prohibitively.

633 In Lemma 9, we have seen that  $x \in \mathbb{R}^d$  lies on the face of some simplex with canonical  
 634 permutahedral representation  $(\tilde{v}_0, \omega)$  in the FK-triangulation if and only if either  $x^i - \tilde{v}_0^i =$   
 635  $x^j - \tilde{v}_0^j$  or  $x^i - \tilde{v}_0^i = 0$  for some  $i, j$ . Note that  $\tilde{v}_0^i, \tilde{v}_0^j \in \mathbb{Z}$ . Hence we see that

636 ► **Lemma 27.** *The Freudenthal-Kuhn triangulation is a hyperplane arrangement  $\tilde{\mathcal{H}} = \{H_{u,k} \mid$   
 637  $u \in E, k \in \mathbb{Z}\}$ , with*

638 
$$E = \{e_1, \dots, e_d\} \cup \{u_{i,j} = e_j - e_i \mid 1 \leq i < j \leq d\}.$$

639 We now define a linear map  $\mu$  from  $\mathbb{R}^d$  to  $P$  by showing how it acts on the basis:

$$640 \quad \mu(e_i) = r_{1,i} = \sum_{i=1}^j s_i.$$

641 We claim that  $\mu$  maps  $E$  bijectively onto  $R_+$ . The vector  $\mu(e_i) = r_{1,i}$  lies in  $R_+$ , by  
642 construction. For  $u_{i,j} \in E$ , with  $i < j$ , we see that

$$643 \quad \mu(u_{i,j}) = \mu(e_j - e_i) = \mu(e_j) - \mu(e_i) = r_{1,j} - r_{1,i} = \sum_{l=1}^j s_l - \sum_{l=1}^i s_l = \sum_{l=i+1}^j s_l = r_{i+1,j}.$$

644 Hence  $\mu(u_{i,j})$  lies in  $R_+$ . By reading the previous calculation backwards we see that  $\mu^{-1}$   
645 maps each  $r \in R_+$  to a vector in  $E$ .

646 We conclude that  $\mu$  (bijectively) maps  $\mathcal{H}$  to  $\tilde{\mathcal{H}}$ , which completes the proof of Lemma 19.  
647

648 We now prove the following:

649 **► Proposition 28.** *The Voronoi cell of a Coxeter triangulation of type  $\tilde{A}_d$  is a permutahed-*  
650 *ron.*

651 **Proof.** We start by recalling a number of results. In [15] we have seen that the circumcentre  
652 of the simplex given in Definition 18 is

$$653 \quad c = \left( -\frac{d-2i}{2(d+1)} \right),$$

654 with  $i \in \{0, \dots, d\}$ . The circumcentre of a Delaunay simplex is a Voronoi vertex. We recall  
655 that

- 656 ■ All simplices in the star of 0 in the Coxeter triangulation are found by consecutive  
657 reflection of the simplex of Definition 18 in the hyperplanes of  $\mathcal{H}$  that go through 0, that  
658 is the hyperplanes with normals  $r_{j,k} = e_j - e_k$ , with  $j \neq k$ . See for example [11, 29, 15].  
659 We also call these reflections the action of the Weyl group.

- 660 ■ The reflection  $R_{j,k}$  in a plane that goes through the origin with normal  $r_{j,k}$  is given by

$$661 \quad R_{j,k}(v) = v - 2 \frac{v \cdot r_{j,k}}{r_{j,k} \cdot r_{j,k}} r_{j,k} = v - (v \cdot r_{j,k}) r_{j,k}.$$

662 We find that

$$663 \quad R_{j,k}(c)^i = (c - (c \cdot r_{j,k}) r_{j,k})^i = -\frac{d-2i}{2(d+1)} - \frac{2j-2k}{2(d+1)} (\delta_{ij} - \delta_{ik}),$$

664 which permutes the  $j$ th and  $k$ th coordinate of  $c$ . Here we used the upper index  $i$  to denote  
665 the  $i$ th coordinate. Using the cycle notation for the permutation group, see for example [4,  
666 Chapter 6], this coincides the 2-cycle  $(jk)$ . Let now

$$667 \quad c_\pi = \left( -\frac{d-2\pi_i}{2(d+1)} \right),$$

668 with  $\{\pi_i\}$  some permutation of  $\{0, \dots, d\}$ . We find that

$$669 \quad R_{j,k}(c_\pi)^i = (c_\pi - (c_\pi \cdot r_{j,k}) r_{j,k})^i = -\frac{d-2\pi_i}{2(d+1)} - \frac{2\pi_j-2\pi_k}{2(d+1)} (\delta_{ij} - \delta_{ik}),$$

670 which again permutes the  $j$ th and  $k$ th coordinate. Now recall that all permutations are  
671 generated by 2-cycles, see for example [4, Theorem 6.1]. This implies that, for any permuta-  
672 tion  $\pi$ , we can find  $c_\pi$  from  $c$  by the action of the Weyl group. This also means that we  
673 have explicitly described the Voronoi cell of 0 in the Coxeter triangulation of type  $\tilde{A}_d$  as a  
674 permutahedron. Because of symmetry, this now holds for any Voronoi cell. ◀

675 **B Proofs for Section 2.1**

676 The proof of Corollary 6 is based on:

677 ► **Lemma 29** (Lemma 3.11 of [33]). *The face of a permutahedron corresponding to an ordered*  
 678 *partition  $\omega = (\omega_1, \dots, \omega_{l+1})$  is combinatorially*

679 
$$\mathcal{P}(|\omega_1|) \times \dots \times \mathcal{P}(|\omega_{l+1}|),$$

680 *where  $|\omega_i|$  denotes the length of the  $i$ th part of the ordered partition and  $\mathcal{P}(k)$  the permuta-*  
 681 *hedron of dimension  $k$ .*

682 **Proof of Corollary 6.** Since the number of vertices of the product of two polytopes is the  
 683 product of the vertices and a  $k$  dimensional permutahedron has  $(k + 1)!$  vertices, we see  
 684 that the total number of vertices of a face of a permutahedron corresponding to an ordered  
 685 partition  $\omega = (\omega_1, \dots, \omega_{l+1})$  is

686 
$$\prod_i (|\omega_i|!).$$

687 Let  $1 \leq k < j \leq d$ , be integers such that  $k + j = d + 1$ . By definition  $k!j! < (k - 1)!(j + 1)!$ ,  
 688 and thus  $k!j! \leq 1!d!$ . Generalizing this, we see that the product of the  $|\omega_i|!$  is maximal when  
 689 all parts are singletons except the biggest part which has  $d + 1 - l$  elements. Therefore

690 
$$\prod_i (|\omega_i|!) \leq (d - l + 1)!.$$

691 ◀

692 **Proof of Lemma 7.** We first recall a set of  $d > 2$  objects can be subdivided in two non-  
 693 empty ordered subsets  $A$  and  $B$  in  $2^d - 2$  ways. This is not hard to see. Because we pick for  
 694 each element if it will be put in  $A$  or  $B$  there are  $2^d$  possibilities. Excluding that  $A$  or  $B$  is  
 695 empty gives  $2^d - 2$ . Let  $\omega = (\omega_1, \dots, \omega_l)$  again be an ordered partition. To find a refinement  
 696 of  $\omega$  in  $l + 1$  parts we need to first pick a  $1 \leq i \leq l$ , such that  $|\omega_i| > 1$  and then we need to  
 697 break  $\omega_i$  up into two (ordered) parts, for which there are  $2^{|\omega_i|} - 2$  possibilities as we have  
 698 seen above. This means that if  $I = \{i \mid 1 \leq i \leq l, |\omega_i| > 1\}$ , the number of refinements is

699 
$$\sum_{i \in I} 2^{|\omega_i|} - 2.$$

700 Let now  $1 \leq k < j \leq d$  be integers such that  $k + j = d + 1$ . Then  $2^k + 2^j < 2^{k-1} + 2^{j+1}$ .  
 701 Generalizing this, we see that the sum of the  $2^{|\omega_i|} - 2$  is maximal when all  $|\omega_i| = 1$  except  
 702 the biggest part which has  $d - l + 1$  elements. ◀